机械与能源工程系
SUSTech Department of Mechanical and Energy Engineering

实 验 报 告

课程名称：机械设计基础

课程编号：ME303

实验题目：The Design of Eight-Leg Crab Robot

学　　号：11810210，11912404，11910335，11810810，11810123，11810314

姓　　名：王思尧，江轶豪，张亭亭，孟子竣，张宇阳，王澍原

专　　业：机器人工程，机械工程，航空航天工程

指导教师：王宏强

实验成绩：

实验日期：2021 年 5 月 1 日

Fundamental of Machine Design

Final Report

Thorough Design, Manufacture & Analysis

Group Member: 王思尧 11810210, 江轶豪 11912404, 张亭亭 11910335,

孟子竣 11810810, 张宇阳 11810123, 王澍原 11810314

0 Summary:

After collecting and consulting some literature, our group formulated three schemes of biped robot, hexapod robot and eight-legged robot. After comparative analysis, the eight-legged robot was finally determined as the scheme of this experiment. After determining the goal, the members of our team first modeled in SolidWorks to determine the design of the body and foot of the eight-legged robot. The body part of the robot is relatively simple, mainly battery, motor and other power transmission parts, and the foot adopts Crane connecting rod. Then the kinematics and dynamics of the foot connecting rod are analyzed by using software such as ADAMS and ANSYS. Finally, a set of parameters with better gait and trajectory are selected. After the end of the simulation stage, the manufacturing process is formally entered. The feet of the first generation of robots were made of aviation laminates with relatively low density and relatively large stiffness, and the main body was mainly made by 3D printing. However, it was found in the test that although the speed of the first generation of robots was relatively fast, the robot trajectory was not straight and would deviate from the predetermined trajectory. Then the robot was optimized by replacing the feet and the body with carbon fiber, which is more rigid, the connecting rod is improved and optimized, and adding synthetic rubber 'shoe covers' to the ends of the feet to increase friction between them and the ground and prevent them from slipping. In the second test, it was found that the running speed was slower than that of the first generation, and the deviation problem still existed. Then, the "shoe cover" at the end was removed to solve the problem of slow speed. At the same time, our team found that the problem of trajectory deviation was caused by the problem of assembling the legs. After correction, the eight-legged robot of our team can now walk on a straight line at a faster speed.

1 Overall Layout & Information of The Crab Robot Based on Klann Mechanism

1.1 Number of Legs

Foot robot generally has two, four, six and eight legs. Differences among types of robots in motion form and function is analyzed.

Biped walking robot is suitable for walking on uneven or obstructed ground. It has stronger flexibility and better mobility than other ordinary mobile robots. However, the biped walking model is a variable structure mechanism, with the single foot support an open chain, and the double foot support a closed chain. The fixation of the support points depends on the friction force to ensure that the mass distribution and weight have a direct impact on the static and dynamic stability. In order to ensure the stability of posture during walking, the gait of walking needs very strict constraints, which is not particularly easy to achieve.

Hexapod robot is also called mimic-spider robot. Hexapod robot is a robot that mainly imitates the limb structure and movement control strategy of insects and other arthropods. Compared with the quadruped robot, the hexapod robot has better stability, because it is easier to meet the spatial stability condition of $\beta \geq 3/2n$, which is very suitable to complete the unstructured and uncertain environment operation. Nevertheless, its limbs have redundancy.

Octa-legged robots are usually designed for specific research purposes on the basis of hexapod robots. They do not have the redundancy characteristics of hexapod robots, while keeping the characteristics of specific bionic creatures. In this experiment, our team selected a crab-like eight-legged robot, consisting of three parts, the foot movement body, the connection structure and the control system. The principal body of the foot movement is the carrier platform of the bionic crab robot, which is mainly composed of two sets of quadruped movement mechanism of gear crank connecting rod and support plate mounted symmetrically. It is driven by the walking stepping motor to realize the basic movements such as transverse walking and steering. The control system is mounted on the principal body of the foot movement. The stepper motor drive module and the steering gear drive module control the rotation Angle and speed of the stepper motor and steering gear by receiving infrared control signals, so as to realize the drive of the corresponding structure.

1.2 The Gait of the Robot

The gait optimization is to stabilize the robot posture and fully deliver the power from the motor. The gait of the robot should allow the robot to maintain standing in every phase of the motion. In this case, we need 4 points to contact the ground at any time. We can divide 8 legs into 2 groups, each group of 4 points contact the ground at the same time in a particular phase of motion. And to maintain the support surface area in two phases to be the same. We design the robot gait as shown below. We call it (2,3,6,7), (1,4,5,8).

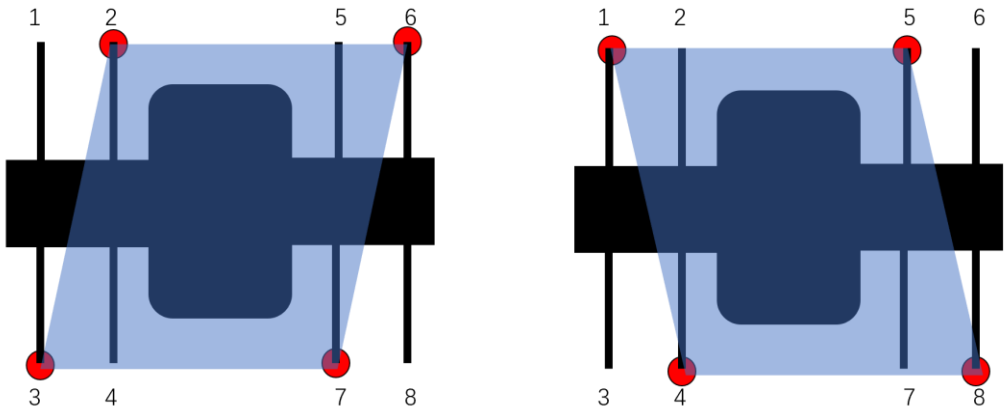

(2,3,6,7), (1,4,5,8) gait & its support polygon

There are other gaits of 8-leg robot as well, including (2,4,5,7), (1,3,6,8). However, the varying area of support polygon of this gait may affect the stability of the robot.

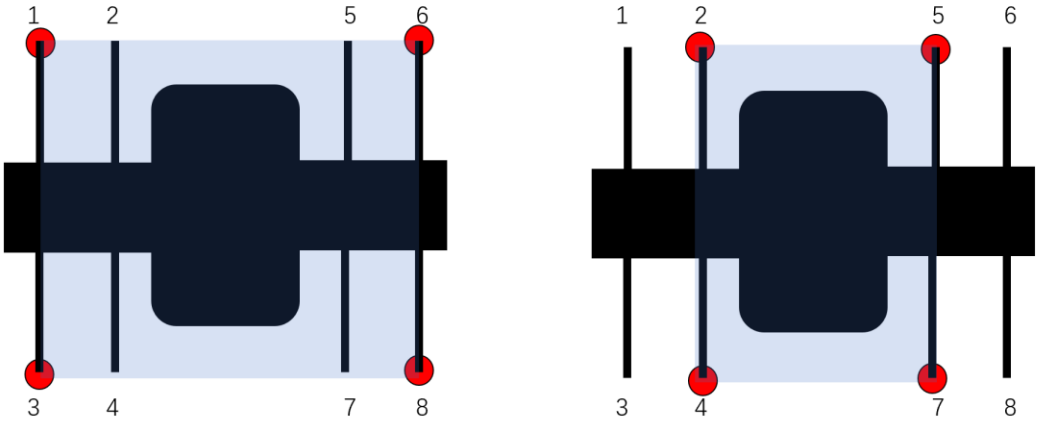

(2,4,5,7), (1,3,6,8) gait& its support polygon

Eventually, we decided to choose the (2,3,6,7), (1,4,5,8) gait to maintain maximum stability of the robot.

1.3 Distribution of Robot Components

To balance the whole body, it is necessary to make the mass distribute uniformly. Basically, the robot is designed as a carb-like structure. The motor is placed in the middle with 8 legs assembled on each side. Battery pack is next to the motor. Both of them are attached to the main body. By this way, mass distribution will be balanced well and the overall structure will be fairly stable. The motor transmits moment of force as source power to rotate the main shaft. The main shaft drives eight legs consequently. Legs are installed to the main body by rotatable linkages. Meanwhile they are linked to the main shaft by gears. On each side, there are four legs moving in the same mode but out of phase.

1.4 Dimensions of Robot & Speed Expectation

The robot size is preliminary decides about 300mm*300mm*200mm. We design the size with reference to the motor. Similarly, depends on the performance of the motor, the speed is expected to be around 0.5~1m/s.

1.5 Plan and arrangement

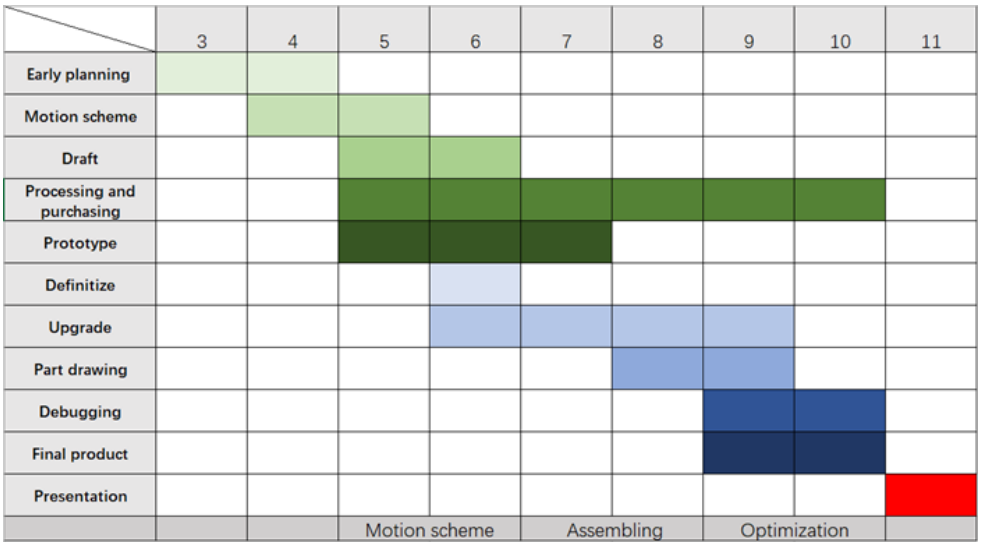

In nine weeks from the third week, we are going to make four generation robots in total, and the main work will be completed in the third generation. First, we need to complete the technical verification and Simulation of the crab robot, and manufacture the first prototype machine. In the sixth week, we need to complete the finalization work. After the final scheme is finalized, we will carry out the debugging, drawing and other work. The focus of work will be on the final optimization. The personnel arrangement is as follows:

Motion analysis and simulation: Jiang Yihao, Zhang Tingting. This work is mainly responsible for verifying the mobility of the robot and providing data support for future optimization.

Mechanical structure design: Zhang Yuyan, Wang Shuyuan, Meng Zijun. This work is mainly responsible for the design, modeling and manufacturing of machine structure.

Drawings and procurement: Wang Siyao. Purchase parts and draw part drawing and assembly drawing.

Optimization: all.

2 Mathematical Analysis of Klann linkage mechanism

2.1 Formulations of the equations of motion for legged robots with closed-loop mechanism

To describe the behavior of a multibody system (MBS) by using the equation of motion, the vector of generalized coordinates for the system can be written as

$$q = [q_1^T \; q_2^T \; \dots \; q_n^T]^T \qquad (1)$$

where $q_i = [x_i \; y_i \; \theta_i]_i^T$ is the vector of planar Cartesian generalise coordinate for an MBS. And for an arbitrary joint *k* between body *i* and body *j*, relative conditions are posed by a kinematic constraint

$$\Phi_k^{K(i,j)} = \left(\boldsymbol{r}_i + \boldsymbol{A}_i \, s_i'^k\right) - \left(\boldsymbol{r}_j + \boldsymbol{A}_j \, s_j'^k\right)$$

$$= \begin{pmatrix} x_i + x_i'^k cos\theta_i - y_i'^k sin\theta_i - x_j - x_j'^k cos\theta_j + y_j'^k sin\theta_j \\ y_i + x_i'^k sin\theta_i + y_i'^k cos\theta_i - y_j - x_j'^k sin\theta_j - y_j'^k cos\theta \end{pmatrix} = 0, \qquad (2)$$

where $\boldsymbol{r}_i$ is the vector to the centroid of the body, $\boldsymbol{A}_i$ is the rotation transformation matrix, and $s_i'^k$ is the local representation of the body fixed vector to point *k*.

According to the configuration of the MBS defined by n vectors of generalized coordinates of $\mathbf{q}$ where *t* is the time, a set of kinematic constraint equations Φ is obtained as

$$\Phi(\mathbf{q}, t) = \begin{bmatrix} \Phi^{\mathrm{K}}(\mathbf{q}) \\ \Phi^{\boldsymbol{D}}(\mathbf{q}, t) \end{bmatrix} = \mathbf{0}, \qquad (3)$$

where $\Phi^{\mathrm{K}}(\mathbf{q})$ is the kinematic constrain equation and $\Phi^{\boldsymbol{D}}(\mathbf{q}, t)$ denotes the driving constraints of the MBS.

The first derivative of Eq. (3) with respect to time is used to obtain the velocity constraint equation while the second derivative of Eq. (3) with respect to time yields the acceleration constraint equation as:

$$\Phi_{\boldsymbol{q}} \dot{\boldsymbol{q}} = \boldsymbol{v}, \quad (4)$$
$$\Phi_{\boldsymbol{q}} \ddot{\boldsymbol{q}} = \boldsymbol{\gamma}, \quad (5)$$

Where $\Phi_{\boldsymbol{q}}$ is the Jacobian matrix of the kinematic constraint equations, $\boldsymbol{v}$ is the velocity equation, and $\boldsymbol{\gamma}$ is the acceleration equation.

Through the virtual power principle, they are shown as:

$$\boldsymbol{M}\ddot{\boldsymbol{q}} + \Phi_{\boldsymbol{q}}^{\boldsymbol{T}} \boldsymbol{\lambda} = \boldsymbol{g}, \quad (6)$$

2.2 The constraints and mathematical model of Klann mechanism

For original Klann mechanism, it is known as the system with 12 links, and an attachment with the ground. The generalized coordinates are defined as follows:

$$\boldsymbol{q} = [\boldsymbol{q_1^T} \; \boldsymbol{q_2^T} \; \boldsymbol{q_3^T} \; \boldsymbol{q_4^T} \; \boldsymbol{q_5^T} \; \boldsymbol{q_6^T} \; \boldsymbol{q_7^T} \; \boldsymbol{q_8^T} \; \boldsymbol{q_9^T} \; \boldsymbol{q_{10}^T} \; \boldsymbol{q_{11}^T} \; \boldsymbol{q_{12}^T} \; \boldsymbol{q_{13}^T}]^T \quad (7)$$

Therefore, 39 ($= 13 \times 3$) elements are obtained in the generalised coordinates in our present analysis. As the equation shown below, the first 38 elements derive from $\Phi^{\mathrm{K}}(\mathbf{q})$ in Eq. (3), and the last element derive from $\Phi^{\boldsymbol{D}}(\mathbf{q}, t)$ which is the driving constraint.

$$\Phi(\mathbf{q},t)=\begin{bmatrix} x_1-l_1\cos\theta_1 \\ y_1-l_1\sin\theta_1 \\ x_2+l_2\cos\theta_2-x_1-l_1\cos\theta_1 \\ y_2+l_2\sin\theta_2-y_1-l_1\sin\theta_1 \\ x_3-l_3\cos\theta_3-x_2+l_2\cos\theta_2 \\ y_3-l_3\sin\theta_3-y_2+l_2\sin\theta_2 \\ x_4-l_4\cos\theta_4-x_3-l_3\cos\theta_3 \\ y_4-l_4\sin\theta_4-y_3-l_3\sin\theta_3 \\ x_7+l_7\cos\theta_7-x_6-l_6\cos\theta_6 \\ y_7+l_7\sin\theta_7-y_6-l_6\sin\theta_6 \\ x_9-l_9\cos\theta_9-x_8+l_8\cos\theta_8 \\ y_9-l_9\sin\theta_9-y_8+l_8\sin\theta_8 \\ x_{11}-l_{11}\cos\theta_{11}-x_{10}+l_{10}\cos\theta_{10} \\ y_{11}-l_{11}\sin\theta_{11}-y_{10}+l_{10}\sin\theta_{10} \\ x_{12}+l_{12}\cos\theta_{12}-x_{11}-l_{11}\cos\theta_{11} \\ y_{12}+l_{12}\sin\theta_{12}-y_{11}-l_{11}\sin\theta_{11} \\ x_4+l_4\cos\theta_4-x_2-l_2\cos\theta_2 \\ y_4+l_4\sin\theta_4-y_2-l_2\sin\theta_2 \\ x_5+l_5\cos\theta_5-x_2+l_2\cos\theta_2 \\ y_5+l_5\sin\theta_5-y_2+l_2\sin\theta_2 \\ x_7-l_7\cos\theta_7-x_4+l_4\cos\theta_4 \\ y_7-l_7\sin\theta_7-y_4+l_4\sin\theta_4 \\ x_8+l_8\cos\theta_8-x_3-l_3\cos\theta_3 \\ y_8+l_8\sin\theta_8-y_3-l_3\sin\theta_3 \\ x_9+l_9\cos\theta_9-x_7-l_7\cos\theta_7 \\ y_9+l_9\sin\theta_9-y_7-l_7\sin\theta_7 \\ x_{10}+l_{10}\cos\theta_{10} \\ y_{10}+l_{10}\sin\theta_{10} \\ x_{12}+l_{12}\cos\theta_{12} \\ y_{12}+l_{12}\sin\theta_{12} \\ x_5-l_5\cos\theta_5-x_{10}+l_{10}\cos\theta_{10} \\ y_5-l_5\sin\theta_5-y_{10}+l_{10}\sin\theta_{10} \\ x_6-l_6\cos\theta_6-x_{12}-l_{12}\cos\theta_{12} \\ y_6-l_6\sin\theta_6-y_{12}-l_{12}\sin\theta_{12} \\ \theta_{11}-\frac{\pi}{2} \\ x_{13}-l_{13}\cos\theta_{13}-x_9+l_9\cos\theta_9 \\ y_{13}-l_{13}\sin\theta_{13}-y_9+l_9\sin\theta_9 \\ \theta_{13}-\theta_9 \\ \theta_1+\omega t \end{bmatrix}=\mathbf{0}\ , \quad (8)$$

And the figure below shows the generalized Klann mechanism, whose linkages have their own x and y coordinate axis for the rotational angle of each joint, and the length of links and other parameters are known, where l_1 to l_{13} are link lengths. However, in our actual project, we will eliminate link BC, link BA, link CD and link CE, replaced by the links, every one of which will have an extra joint, and the shapes can be designed like a triangular. (Both transformations are equivalent and cannot modify the degree of freedom).

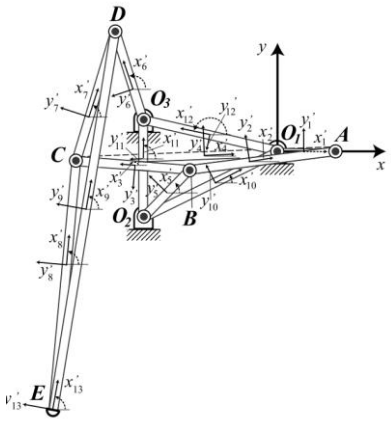

Fig. Generalized coordinates on the Klann mechanism

2.3 Optimization Technique

Step height and stride length are the two most important parameters of the foot locus, which are the consideration and targets of the optimization. Higher the step height, better will be the all−terrain capability to overcome obstacles, also, longer the stride length is, faster the robot finishes the same displacement. Therefore, the objective of the optimization is to maximizing the coordinates of step height (x_{sh}, y_{sh}) and stride length (x_{sl}, y_{sl}).

$$Max(x_{sh}, y_{sh}, x_{sl}, y_{sl}) = f(\theta_{in}, l_1, l_2, l_3 \dots l_n) \quad , (9)$$

Now we use this figure as a sample of modelling, considering a close-loop equation for loop ABDC.

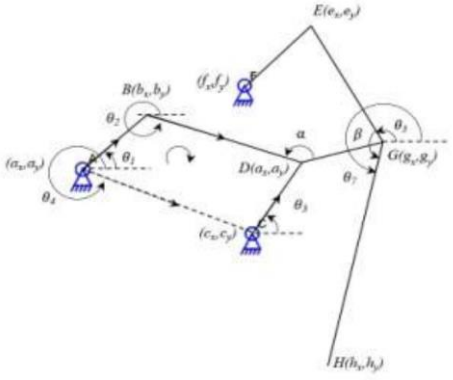

Fig. Kinematic representation of Klann's linkage

$$\overrightarrow{r_1} + \overrightarrow{r_2} - \overrightarrow{r_3} - \overrightarrow{r_4} = 0 \text{ , } (10)$$

$$r_1 e^{i\theta_1} + r_2 e^{i\theta_2} - r_3 e^{i\theta_3} - r_4 e^{i\theta_4} = 0 \quad , (11)$$

$$r_1(cos\theta_1 + isin\theta_1) + r_2(cos\theta_2 + isin\theta_2) - r_3(cos\theta_3 + isin\theta_3) - r_4(cos\theta_4 + isin\theta_4) = 0 \quad , (12)$$

Then locating the coordinates of Point D

$$d_x = r_1 cos\theta_1 + r_2 cos\theta_2 = acos\theta_1 + bcos\theta_2 \ , (13)$$
$$d_y = r_1 sin\theta_1 + r_2 sin\theta_2 = asin\theta_1 + bsin\theta_2, (14)$$

Then there is the position analysis of output link GH

$$h_x = g_x + gcos\theta_7, (15)$$
$$h_y = g_y + gsin\theta_7, (16)$$

2.4 Simulation results and analysis

Table.1 Link Length & Foot Locus Parameters of Klann Mechanism.

Link	*Iteration Result 1(mm)*	*Iteration Result 2(mm)*	*Iteration Result 3(mm)*
1	137.1	84.9	110.2
2	64.2	39.5	77.4
3	88.6	63.2	68.4
4	226.8	150.3	150.3
5	122.7	99.5	99.5
6	347.9	241.0	240.9
7	84.3	55.3	55.3
8	102.8	56.4	56.4
9	133.3	96.9	102.9
10	234.8	151.4	159.4
11	60.2	49.2	49.2
12	50.9	36.0	26.0
Result	Stride Length: 276.12mm Step Height: 242.8mm	Stride Length: 218.2mm Step Height: 56.74mm	Stride Length: 74.18mm Step Height: 73.41mm

Stride Length: Model 1 > Model 2 > Model 3
Step Height: Model1 > Model 3 > Model 2

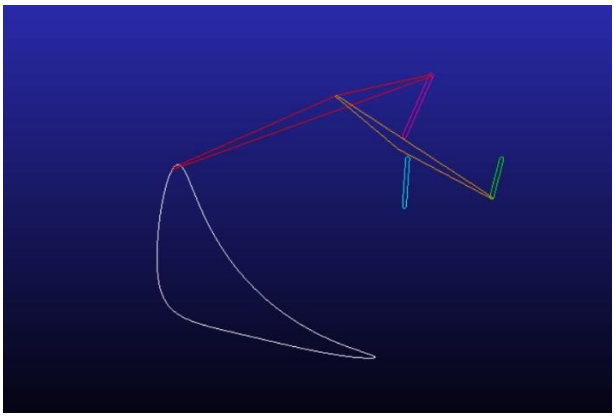

(a)

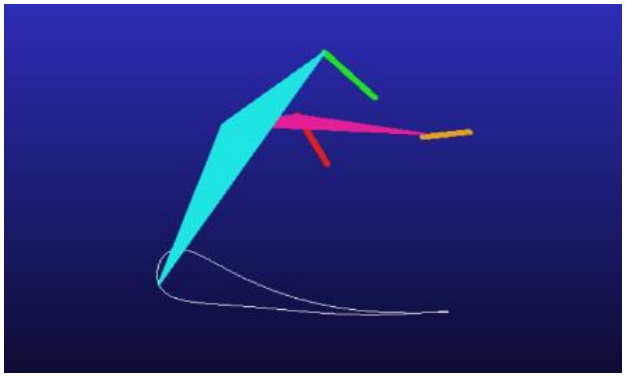

(b)

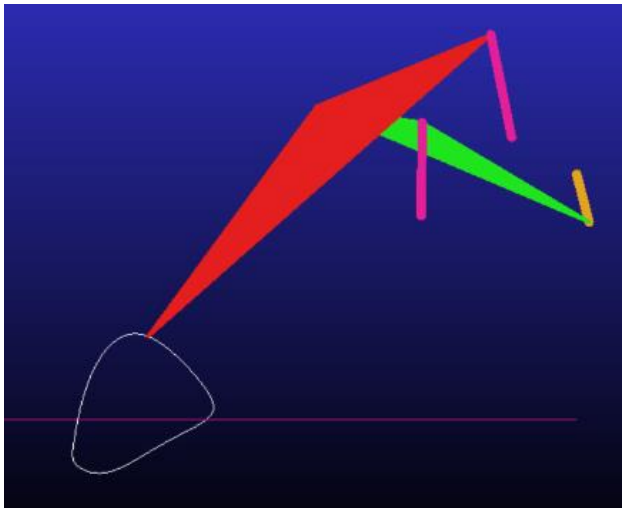

(c)

Fig. (a) (b) (c) Foot trajectories obtained using ADAMS for results 1, 2 & 3 respectively

In order to determine which iteration result is the most suitable one, step height and stride length should be concerned. For the comparison, step height will weigh less, because the target of the competition is to reach the destination in a faster speed and stability is more important, which pose a challenge to us to reduce the displacement change of gravity center during the march in one period. Also, the optimization of the magnitude velocity, is to be more stable to

have a better command of phase control.

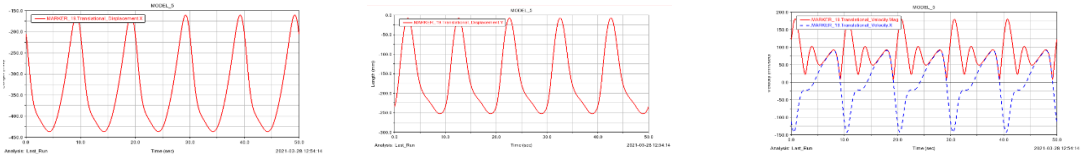

(a) (b) (c)

Fig.4 (a) (b) (c): Displacement on x & y axis & the velocity of model 1

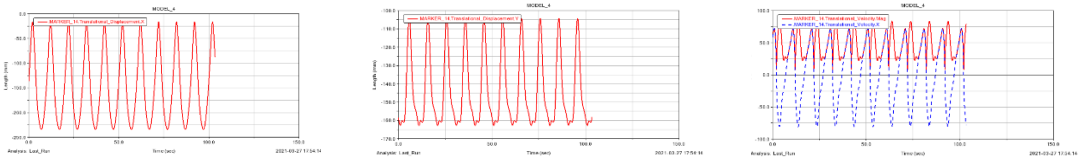

Fig.5 (a) (b) (c): Displacement on x & y axis & the velocity of model 2

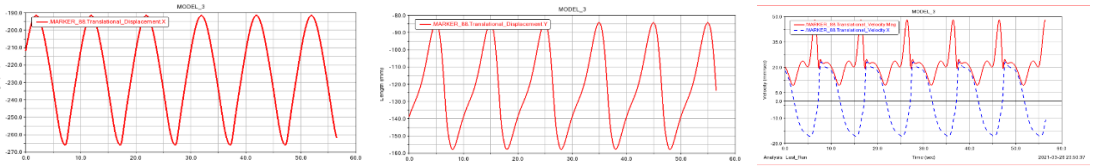

Fig.6 (a) (b) (c): Displacement on x & y axis & the velocity of model 3

Table.2 The magnitude of velocity change of different models

Model #	Speed Change (mm/s)
Model 1	132.0
Model 2	72.1
Model 3	42.3

Velocity Change: Model 1 > Model 2 > Model3

2.5 Conclusion on Motion Analysis

Stride Length: Model 1 > Model 2 > Model 3

Step Height: Model 1 > Model 3 > Model 2

Speed Change: Model 1 > Model 2 > Model3

Through estimating the overall performance of each link parameter, The link model 2 became our option of the solution.

2.6 Fabricated Prototype

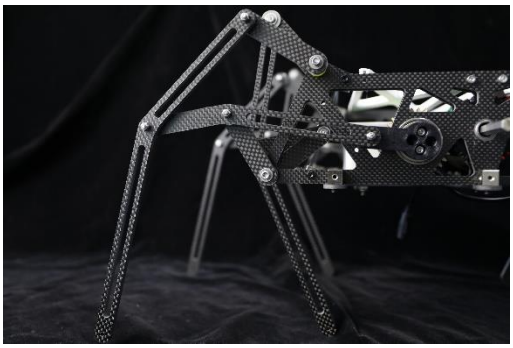

Fig. Fabricated Prototype of Leg Design

3 Simulation & Calculation

3.1 Torque Analysis

We conducted an analysis of the relation between the foot end force and the torque of the transmission shaft. The robot's eventual weight is about 1kg. There are 4 legs contact with the ground at a time. Therefore, approximately divided by 4, we applied a 3 newtons force on one of the foot end vertically to simulate the gravity force. Another force of friction of 0.15N is also applied to the foot end. The torque curve of the shaft is shown below.

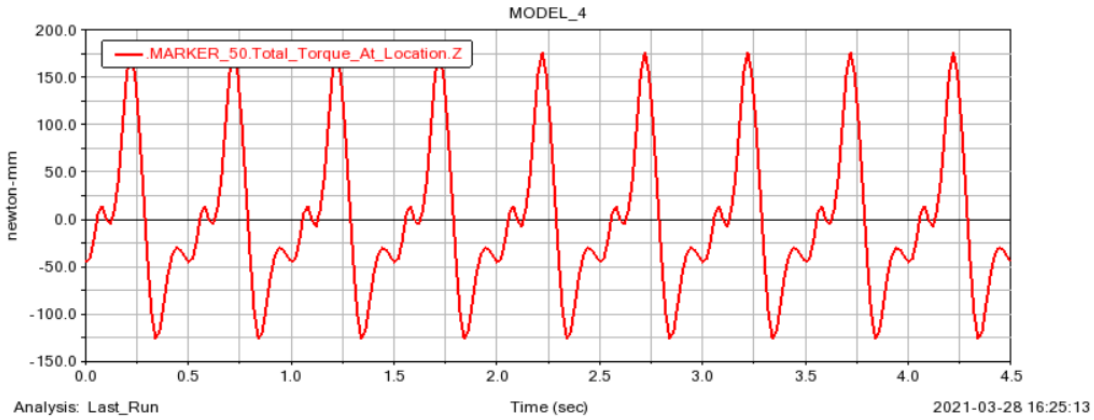

Through this curve, the maximum torque is about 0.176N·m, which determines the torque that one leg delivers to the shaft. There are 4 legs making contact with the ground at any time. The summed torque is 0.704N·m, which is below the output Torque of the motor. By applying a safety factor of 2, the output shaft should sustain a torque of 1.4N·m. Therefore, the transmission rate is determined no more than 1:0.7.

3.2 Power & Motor

The battery pack has a male input charging wire and a female output wire. Both of them are 5.5*2.1mm connector. Use a couple of adapters with wires to connect the output connector of the battery to the motor pins. The wires are welded to the pins of the motor.

The properties of motor and battery are listed as followed:

Motor properties	
Mass	192.5g
Input voltage	24V
Scale	See sketch below
Revolution speed (empty load)	300r/s
Current (empty load)	0.13A

Revolution speed (full load)	245r/s
Current (full load)	0.62A
Rated moment	2Nm
Stall moment	20Nm
Stall current	2.19A
power	10W
Reduction ratio	16.6

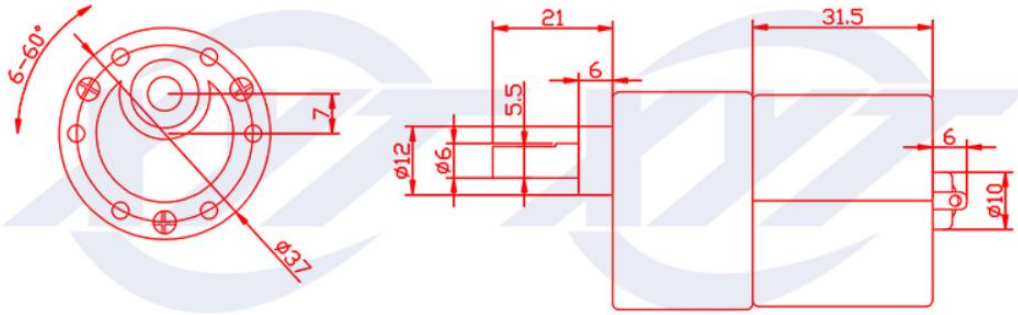

Battery pack properties	
Mass	389.5g
Voltage (output)	24V
Current	4A (stable) 10A (maximum)
Capacity	300mAh
Scale	132*68*49mm
Charging voltage and current	25.2V 1A

3.3 Transmission Ratio

As for transmission device, we chose a simple scheme, the motor will drive Gear1, which connected with Gear2 and drive the Main drive shaft, then the drive shaft can drive the robot. Gear1 is spur gear with keyways and screw holes to connect with motors, and Gear2 is spur gear with hexagonal hole connects with the shaft. Gears is made of stainless steel. And the shaft is hexagonal, two ends of the shaft connect with gears that can drive the robot. The shaft is still made of stainless steel. The motor will be arranged horizontally. The advantages of this transmission mode are simple structure, easy to dismantle and inspect, small transmission loss and low cost of course. Since the robot will be made of aviation laminated plate, it will be light, so the stainless-steel shaft is basically not bearing payload force.

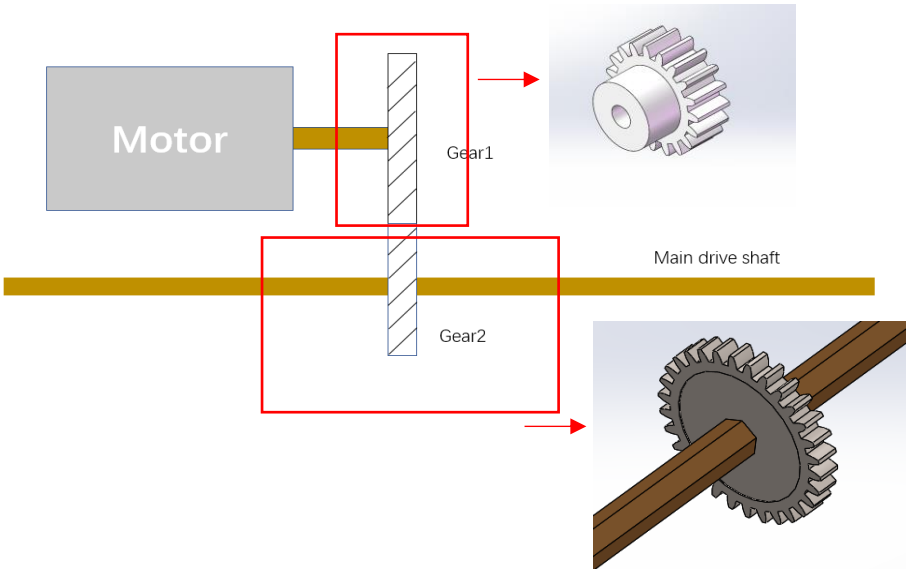

The pictures below show the deformation and stress of the shaft, Because stainless steel has good mechanical properties, So the force exerted by the robot has little effect on the shaft, the largest deformation on the shaft is no more than 0.2mm. The stress distribution of the shaft is relatively uniform, and the maximum stress is about 700MPa, the average stress is about 600 MPa.

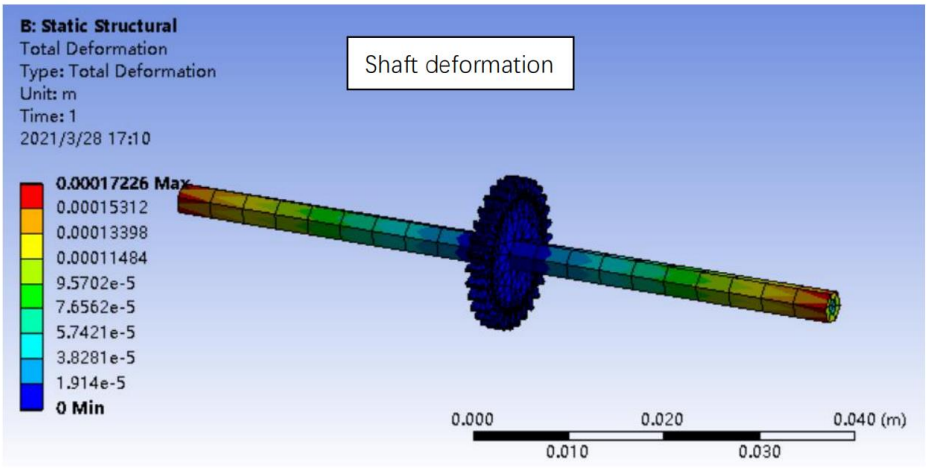

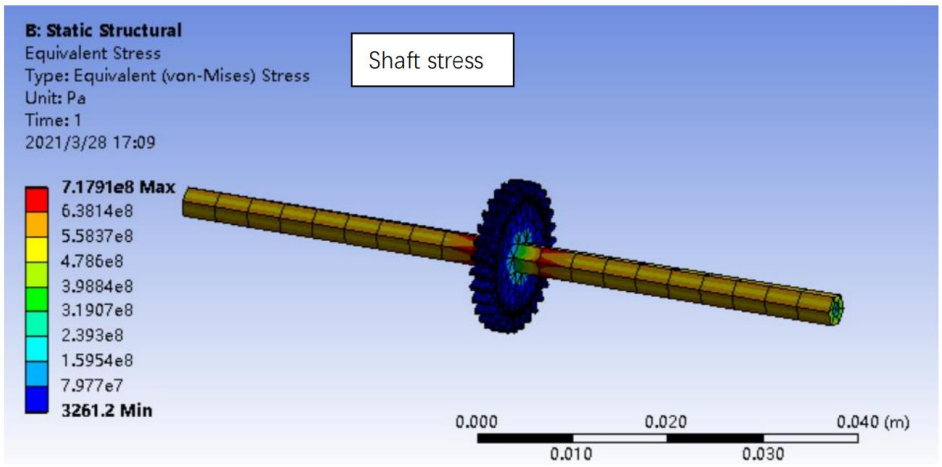

Fig. Stress Simulation

3.4 Gear selection

Through searching on the Internet, we found several suitable motor boss gears, whose parameters are shown in the table below:

The gear selection				
serial number	modulus	pitch diameter/mm	number of teeth	diameter of bore
1	0.5	7.5	15	6
2	0.5	12.5	25	6
3	0.5	17.5	35	6
4	1	15	15	6
5	1	25	25	6
6	1	35	35	6
7	1.5	22.5	15	6
8	1.5	37.5	25	6
9	1.5	52.5	35	6

Our design is to try through gears of different sizes but with the same diameter sum of the reference circle, and finally get a gear combination with higher speed and stability.

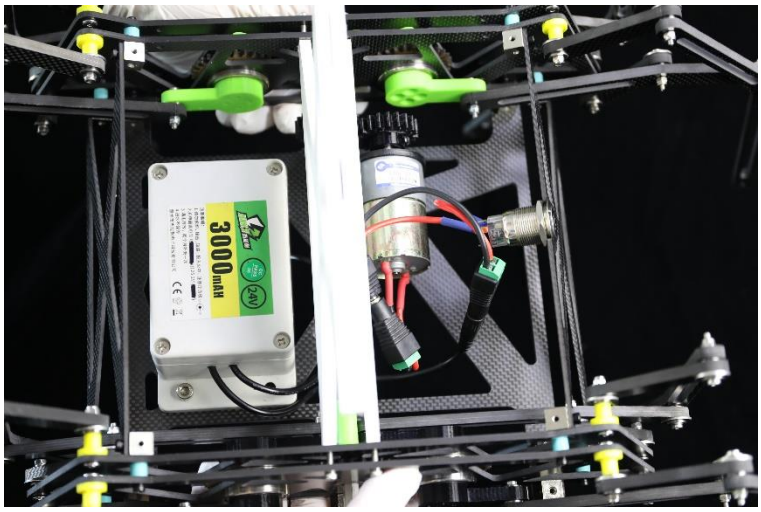

Fig. Gear and Transmission System

4 CAD Design of The Crab Robot

It is essential to build a 3D CAD model in a virtual environment in advance to validate the idea and link with the manufacture process. In this project, SolidWorks is used as the 3D CAD tool to help with designing.

The Robot is mainly made of 3D printed material, PLA. Enabling the robot component to have a better degree of freedom in designing. The assembly graph and some of the engineering drawings are shown below.

4.1 Assembly Drawing

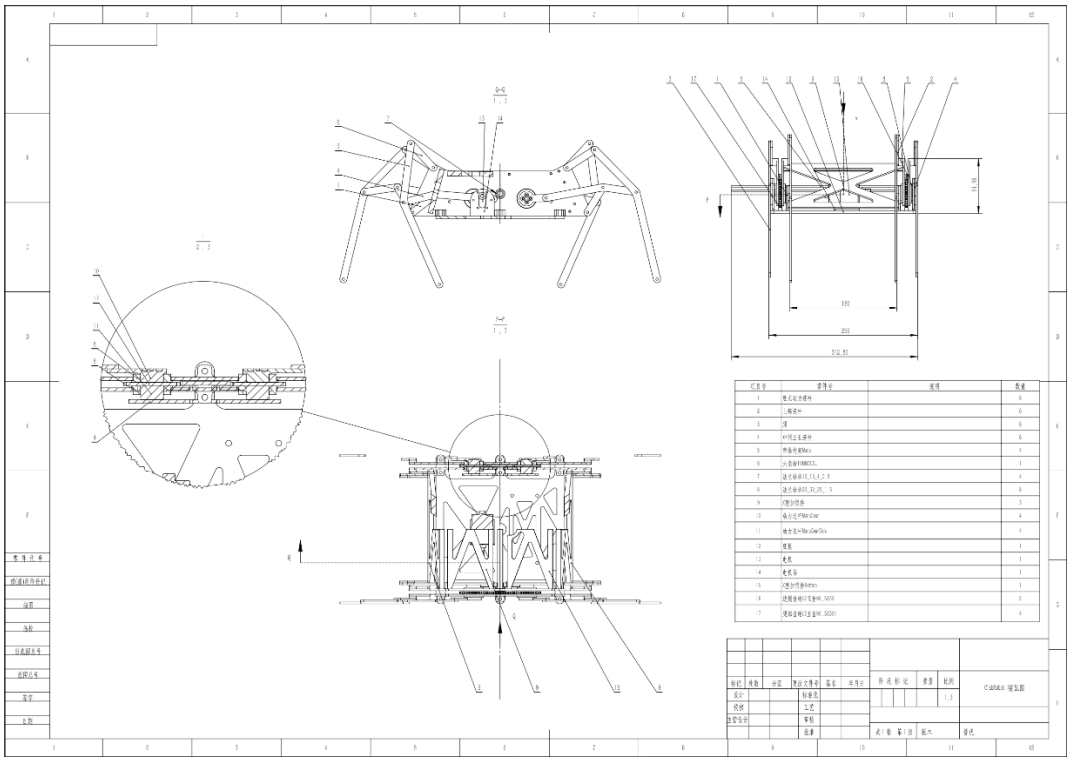

4.2 Engineering Drawings

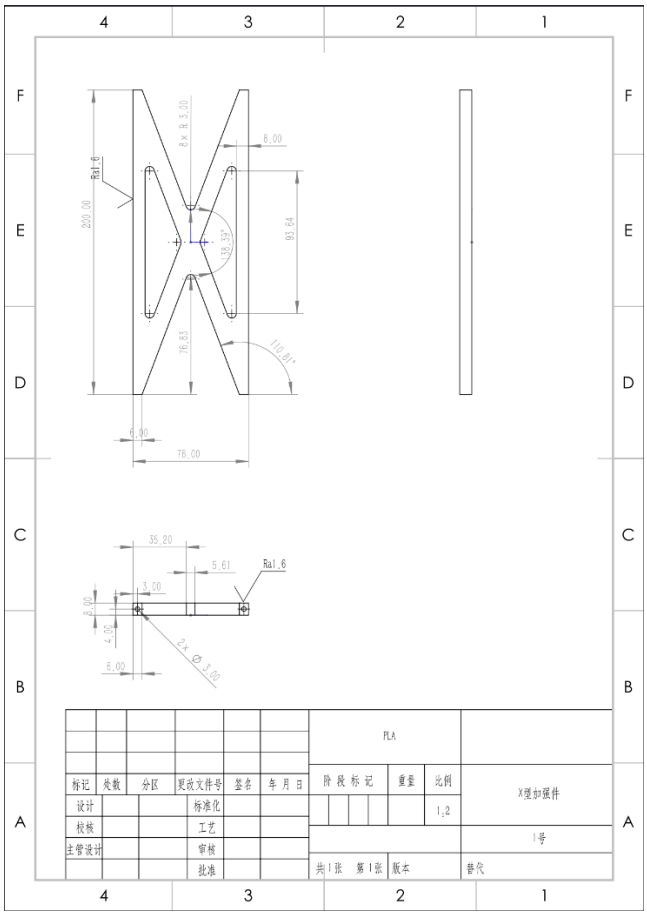

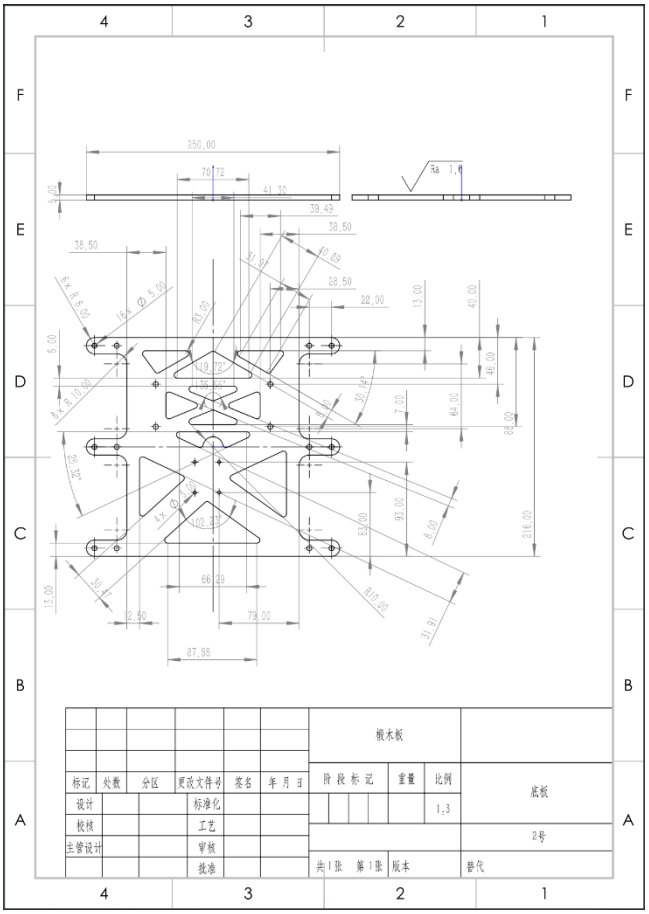
4
3
2
1
F
E
D
C
B
A
250.00
70.72
41.30
39.49
38.50
38.50
28.50
22.00
13.00
40.00
46.00
64.05
88.00
216.00
93.00
63.00
8.00
66.39
79.00
87.88
12.50
13.00
Ra 1.6
底板
比例
1:3
2号
共1张 第1张
版本
替代
标记 处数 分区 更改文件号 签名 年月日
设计
校核
主管设计
标准化
工艺
审核
批准
阶段标记 重量

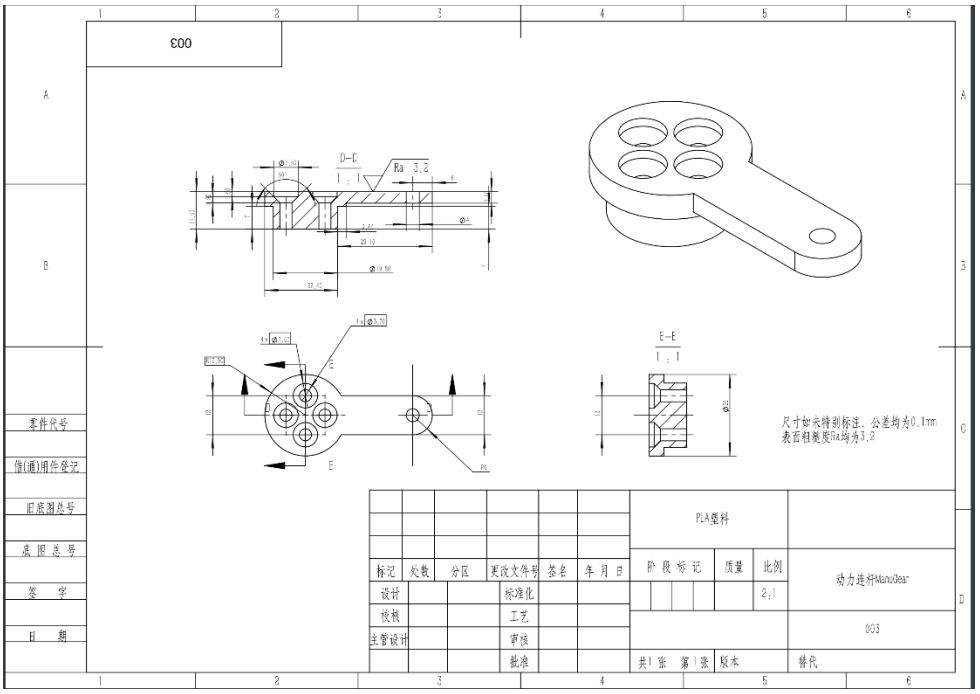
003
D-D
1 : 1
Ra 3.2
E-E
1 : 1
尺寸如无特别标注，公差均为0.1mm
表面粗糙度Ra均为3.2
PLA塑料
比例
2:1
003
共1张 第1张
版本
替代
标记 处数 分区 更改文件号 签名 年月日
设计
校核
主管设计
标准化
工艺
审核
批准
阶段标记 质量
零件代号
借(通)用件登记
旧底图总号
底图总号
签字
日期

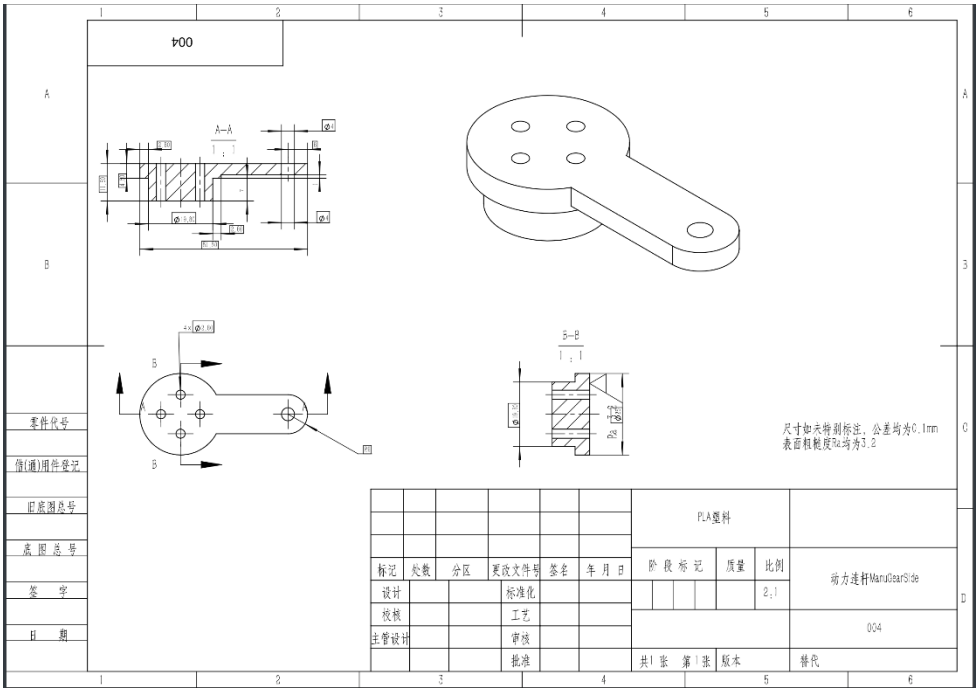
004
A–A
B–B
尺寸如无特别标注，公差均为0.1mm
表面粗糙度Ra均为3.2
PLA塑料
动力连杆ManuGearSide
004
共1张 第1张
版本
替代

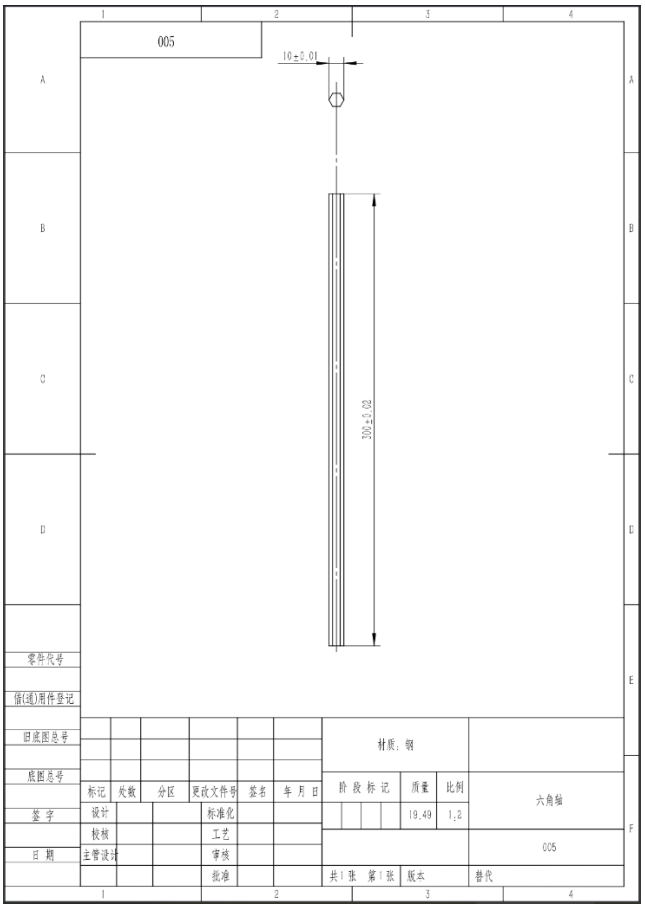
005
10±0.01
300±0.02
材质：钢
六角轴
005
共1张 第1张
版本
替代

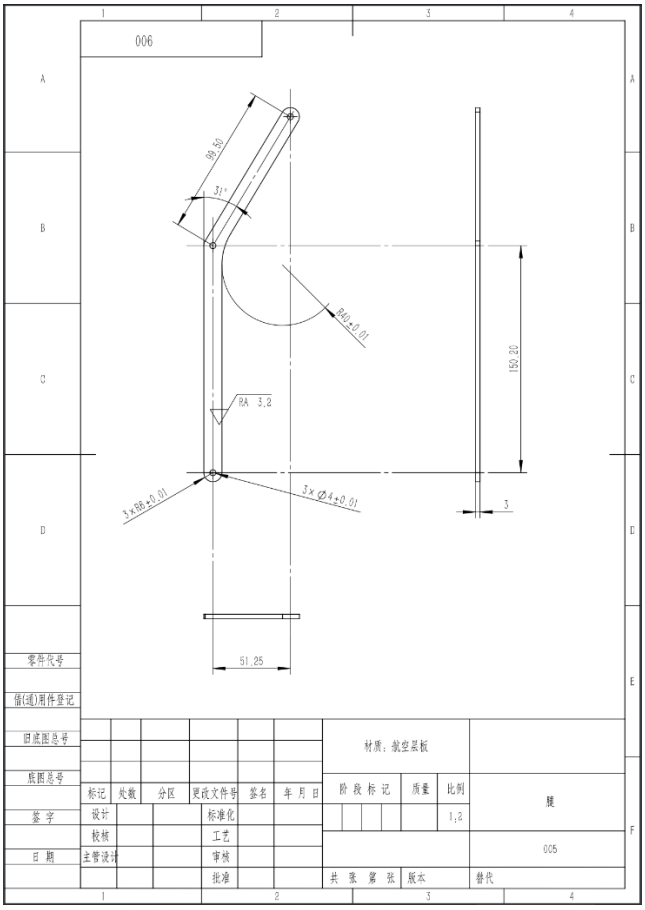

5 Manufacture of The Robot

Manufacture of the robot mainly uses 3D printing and laser cutting, which is able to thoroughly implement mechanical design. The manufactured prototype is shown below.

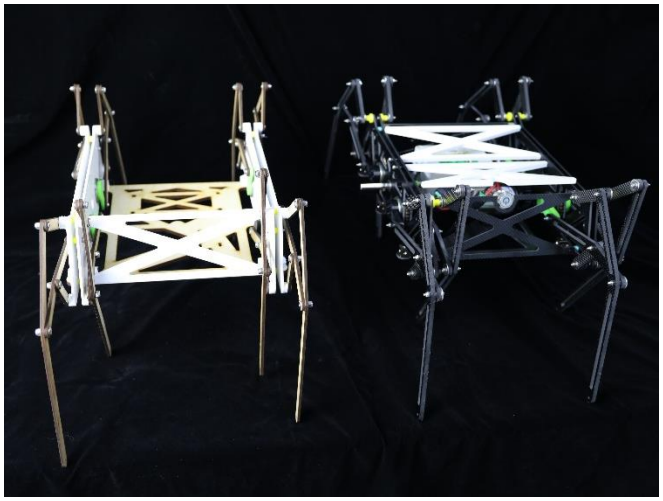

Fig. Manufactured Prototype and Second Generation

In first edition, shanks of locomotion robot are produced by transferring CAD drawing to laser cutting machine, which slices components from an

aeronautical laminate. Joints are linked by bolts temporarily. Entire body and gears are made by 3D printer, performing strong stiffness and high compatibility. To be mentioned, owing to the poor stiffness of the shaft, a new fastener is fabricated by 3D printer. It can match the holes on body accurately and fix the shaft firmly.

In second edition, carbon fiber is introduced to strengthen the stiffness of the robot. Aeronautical laminate and 3D print material is replaced. Meanwhile, flange bearings are used instead of bolts to link joints, delivering less friction.

6 Current Problems & Desirable Adjustment

6.1 Defects of first edition

6.1.1 Stiffness Problem of the 3D Printed Shaft

When applied force or torque on the gear on the shaft, the shaft will move fromits original position due to poor stiffness of the shaft. Causing the increase of distance between gears. Eventually causing the slipping of gears.

6.1.2 Friction Between Links Using Bolt & Nut Connection

Using the bolt nut connection between the links is easy to assemble and light weight. But the friction is increased when tightening the bolts, causing the robot to lose power.

6.1.3 Axial Spacing of the Center Shaft

In the first-generation design, the shaft is not entirely fixed axially but free to move. The only force holding the shaft in its position is friction force. The shaft will gradually deviate from the center position and causing the gear to be disengaged.

6.1.4 Unstable motion

In the initial design, because the stiffness of legs is not enough, it will swing in motion, increasing the gap between legs, and the center of gravity of the robot is on the left, so it will be unable to walk in a straight line, and will continue to yaw to the left.

6.2 Further Iterations & Upgrades

6.2.1 Material Upgrades

In original edition, we use aeronautical laminate, made of birch and basswood, as major material throughout the whole design. Compared with normal materials, specifically, metal and acrylic, its relatively light weight and high stiffness is of our interest.

Taking advantages of aeronautical laminate into consideration, we find carbon fiber, a widely used aeronautical material, seem to be an alternation. In domains of weight and stiffness, carbon fiber has a much better performance than aeronautical laminate. Meanwhile, other advantages including high tensile strength, high chemical resistance, high temperature tolerance and low thermal expansion expand working limitation in extreme and unexpecting environments.

Fig. Aeronautical Laminate

Fig. Carbon Fiber Plate

6.2.2 Linkage Upgrades

We develop two ways to optimize the linkage of our robot.

During our further experiment, we can observe and simulate proper ration between gaits and gears, through which our robot can maintain high velocity while outputting applicable torque to overcome rough walking condition.

In other aspect, we first use normal joint design, which is composed of bolts and nuts. However, such combination could provide quite high frictional considering large quantities of joints. Hence, we can use flange bearings and thrust bearings to form joints in order to eliminate vast friction. However, the high weight of such bearings, especially multiplying large number of joints, is another problem we need to face.

Fig. Flange Bearings

6.2.3 Control System

Our robot is only capable of one-dimension motion. Therefore, it is of great importance to develop control system to achieve higher dimension missions.

First and foremost, we can design H-bridge circuit to achieve forward and backward motion.

On the other hand, we can develop swarm robot system to control a group of walking robots, which implies a promising application potential.

6.3 Update results

6.3.1 Main structure

In the original design, the main part of the robot is made of pla3d printing, which is heavy. In the new design, the main structure is made of carbon fiber plate, and hollowed out, which reduces the weight and greatly enhances the strength of the main structure.

Fig. Solidworks model

6.3.2 Legs

The legs are also made of carbon fiber board and hollowed out treatment to reduce weight. The joints are connected by flange bearings, which greatly reduces the friction between movements. The leg board is double-layer, which can not only increase the stiffness, but also avoid the leg shaking, and

ensure that the movement track is straight.

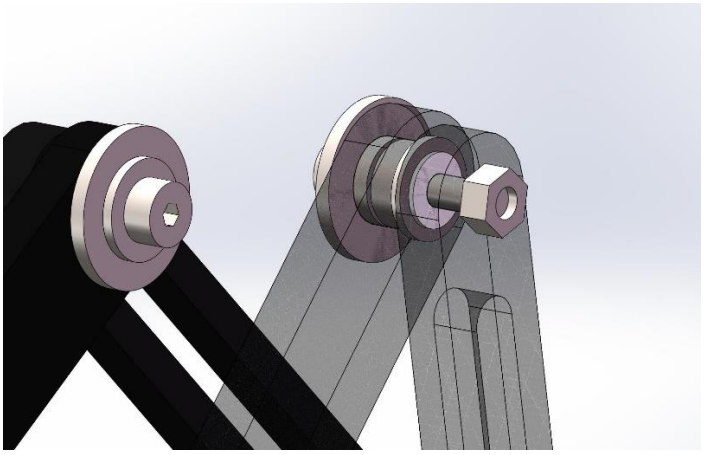

Fig. Bearing

6.3.3 Shoe cover

In order to increase the friction between robot and smooth ground and speed up the walking speed, a kind of shoe cover is designed. The shoe cover is made of synthetic rubber and is placed on the bottom of the robot foot. However, after the test, it is found that the increase of shoe cover will reduce the travel speed because of the great increase of friction, so it is cancelled in the final scheme.

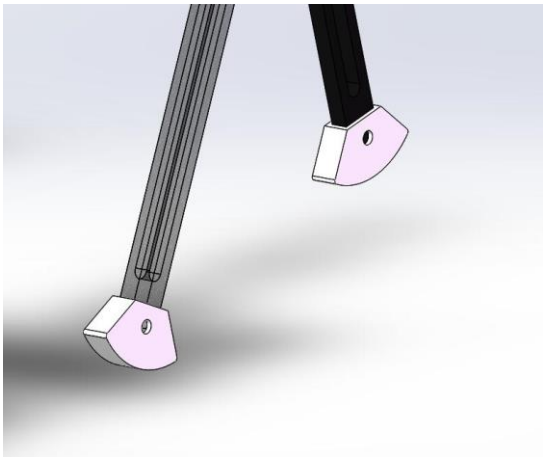

Fig. Shoe cover

7 Final design

The final design of the robot remains the same 8-feet layout and the same gaits as the first generation. The motor and the battery are placed in the central cabin of the robot, separated by the central transmission shaft. The motor output the torque to the transmission shaft through a 20-20 gear set. The transmission shaft then transmits torque to the side gear of each leg module with a 30-30 gear set. The crank mechanism then feed the power to the leg mechanism.

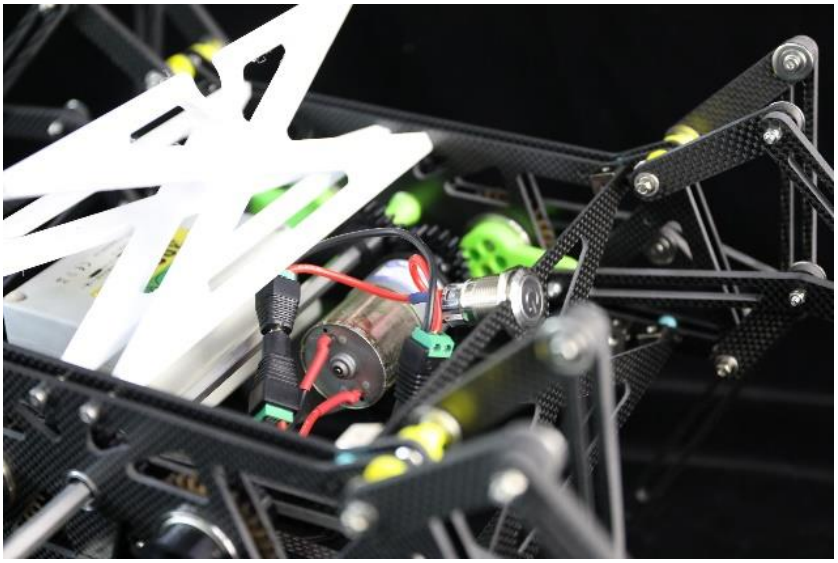

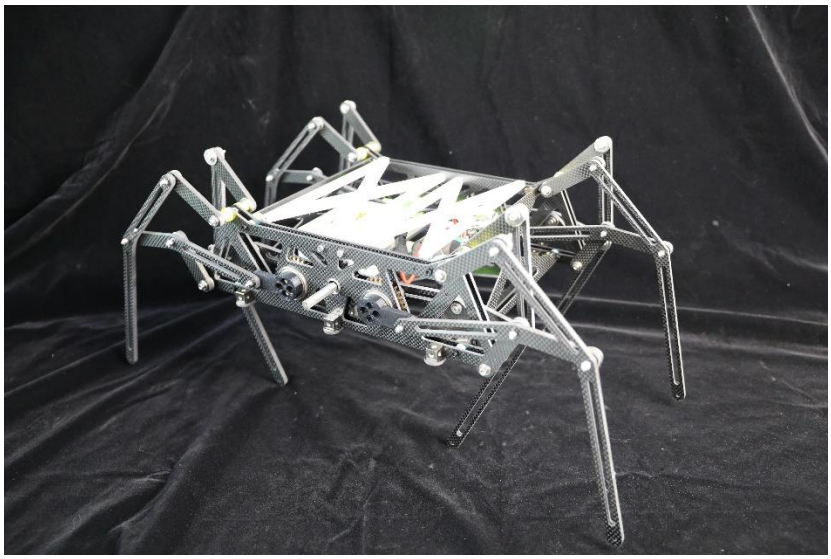

Fig. Internal and Overall Design of the Robot

In the final version, we used carbon fiber plate for the main body material of the robot in order to maintain a good stiffness of the robot body and durability. Due to the outstanding properties of carbon fiber, we can dramatically reduce the weight of the final robot by making hollow lightening holes on the carbon fiber plate.

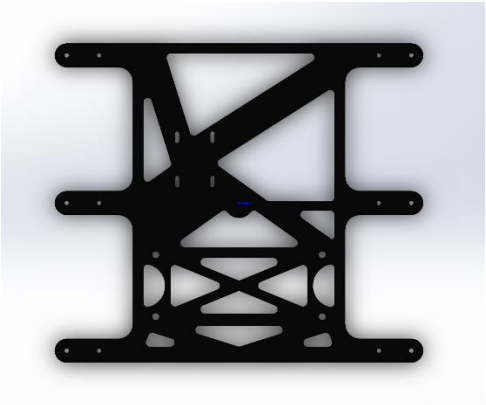

Fig. The hollow out design of carbon fiber plate.

Apart from the material upgrade, the joint at each hinge of the robot legs is designed to be frictionless using flange bearings. The bolts and screws are used to hold the bearings and the leg plates together and plenty of washers are used to prevent potential rubbing between leg plate and the bearings.

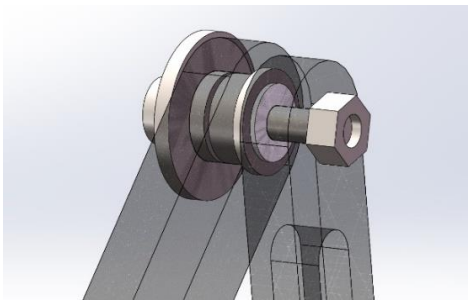

8 Conclusion

In this report, our group has developed a single-motor-actuated walking robot with eight legs capable of fast walking and maintaining a good stability. First, we build a mathematical model of a six-linkage mechanism revealing the motion trajectory of the end of leg. Motion analysis using MATLAB and Adams provides with the information of kinematics and dynamics including the velocity and acceleration of the joints and the torque of the driving shaft, and the parameters of the trajectory including the stride length and step height. Second, the DC motor is determined according to the torque required simulated by Adams and the parameters of transmission system composed of gears and a hex roller is also determined. Third, the model of the robot is designed by SOLIDWORKS and it is tested by SOLIDWORKS motion module. The materials are also determined according to the dynamic analysis. Finally, the walking robot is assembled and tested on the flat floor.

There are two generations of our products. The differences of two robots are the material of the hex roller and its eight legs, joints of linkages on the legs and the antiskid covers on the foot. For the first generation, the material of the hex roller is made of PLA and the leg is made of aviation laminate, both of which lack a good stiffness to bear a quick motion and a large stress. Therefore, for the second generation, the roller is made of steel and the legs are made of carbon fibre. To ensure a better rotation, the second-generation robot uses bearing instead of using screw directly in the first-generation robot. Besides, to magnify the friction between the foot ends and the ground, the antiskid covers are designed. The walking robot designed by our group has shown good properties including the speed of walking and stability during the walk on a straight line and stability of the gravity centre by reducing the step height.

9 References:

[1]. 基于齿轮传动的结构仿生螃蟹机器人设计　秦慧斌，郑智贞;

[2].仿螃蟹机器人步行运动平稳控制及仿真分析　王珏

[3].仿蟹机器人步态规划及复杂地貌行走方法研究 王刚

[4]. Pratik Walimbe. (2018). EFFECT OF VARIATION OF ANGLES OF TERNARY LINKS ON THE GAIT PATTERN OF KLANN'S MECHANISM. International Journal of Research in Engineering and Technology, 7(8), 126-131.

[5]. Komoda, Kazuma, & Wagatsuma, Hiroaki. (2017). Energy-efficacy comparisons and multibody dynamics analyses of legged robots with different closed-loop mechanisms. Multibody System Dynamics, 40(2), 123-153.

[6]. Sheba, Jaichandar Kulandaidaasan, Elara, Mohan Rajesh, Martínez-García, Edgar, & Tan-Phuc, Le. (2017). Synthesizing reconfigurable foot traces using a Klann mechanism. Robotica, 35(1), 189-205.